MULTI-MODAL ACTION RECOGNIZER BRIDGES HUMAN MOTION GENERATION AND UNDERSTANDING

Anonymous authors
Paper under double-blind review

ABSTRACT

Human action recognition and motion generation are two active research problems in human-centric computer vision, both aiming to align motion with textual semantics. However, most existing works study these two problems separately, without uncovering the bidirectional links between them, namely that motion generation requires semantic comprehension. This work investigates unified action recognition and motion generation by leveraging skeleton coordinates for both motion understanding and generation. We propose Coordinates-based Autoregressive Motion Diffusion (CoAMD), which synthesizes motion in a coarse-to-fine manner. As a core component of CoAMD, we design a Multi-modal Action Recognizer (MAR) that provides semantic guidance for motion generation. Our model can be applied to four important tasks, including skeleton-based action recognition, text-to-motion generation, text–motion retrieval, and motion editing. Extensive experiments on 13 benchmarks across these tasks demonstrate that our approach achieves state-of-the-art performance, highlighting its effectiveness and versatility for human motion modeling.

1 INTRODUCTION

Human-centric computer vision (Wang et al., 2025b; Tang et al., 2025) aims to understand, interpret, and interact with humans through visual data, encompassing tasks such as person search, human pose estimation, action recognition and attribute recognition. Human motion modeling, a key area of human-centric research, aims to represent, understand, predict, and generate human movements, with applications in animation, virtual avatars, behavior analysis, and human–robot interaction.

Early research in human motion modeling primarily focuses on understanding human actions, particularly skeleton-based action recognition. Representative approaches include hierarchical modeling (Du et al., 2015), which represents actions at multiple levels of spatial granularity; spatio-temporal modeling (Yan et al., 2018), which captures both the spatial configurations and temporal dynamics of the human body; and the two-stream paradigm (Wang & Wang, 2017; Zhu et al., 2023a), which learns representations with separate spatial and temporal streams to enhance action understanding. Although action understanding associates human motion with semantic labels, these semantics are constrained by a limited number of action classes.

With the rapid development of text-to-image generation (Ramesh et al., 2022; Saharia et al., 2022), generating human motion from textual descriptions has gained increasing attention (Zhu et al., 2023b). Text-to-motion generation aims to synthesize realistic and semantically consistent human motions conditioned on natural language, bridging the gap between high-level semantic understanding and low-level motion dynamics. Methods based on diffusion models (Tevet et al., 2023; Zhang et al., 2024a), autoregressive transformers (Pinyoanuntapong et al., 2024a), and large language models (LLMs) (Jiang et al., 2023) have been successfully applied to text-to-motion generation. While existing diffusion-based and autoregressive approaches effectively capture temporal dependencies and generate realistic, smooth motions, they are primarily designed for one-way text-to-motion generation and are less capable of handling motion-to-semantic tasks.

Although skeleton-based action recognition and text-to-motion generation are two important tasks of human motion modeling. Most existing works study the two tasks separately, without exploring their potential connections. However, these two areas are inherently connected, as they both build alignment between motion dynamics and textual semantics. Action understanding provides structured

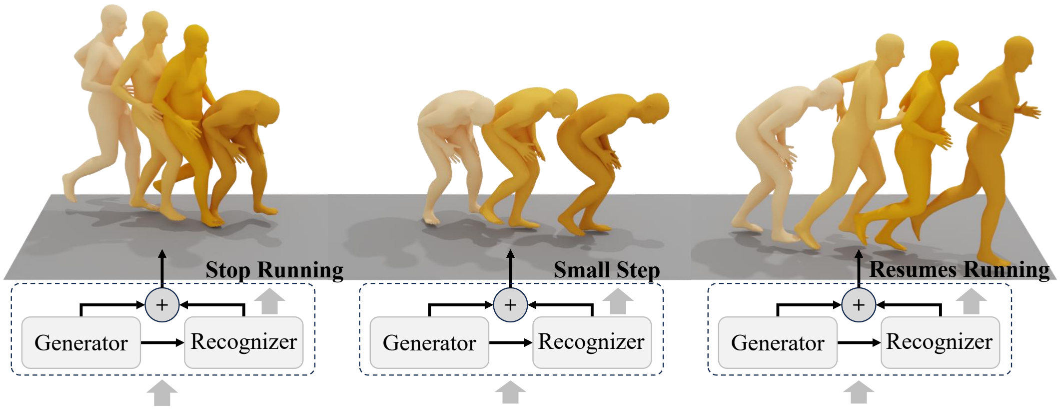

Figure 1: Our framework operates in an iterative loop where a Generator synthesizes a portion of the motion, and a Recognizer facilitates its semantic alignment with the text. The recognizer's feedback guides the generator's next step, progressively refining the motion to match complex descriptions.

knowledge of motion dynamics and semantics, which can guide controllable generation; conversely, generative models capture rich motion priors that can enhance recognition through data augmentation and spatio-temporal modeling. Bridging the gap between understanding and generation not only enables a unified framework for bidirectional tasks such as motion-to-text and text-to-motion, but also fosters more robust and generalizable human motion modeling.

In this work, we propose a novel framework that bridges the gap between motion generation and action recognition. Our core idea is to leverage a well-trained Multi-modal Action Recognizer (MAR) not merely as a recognition tool, but as an active semantic guide within the generative process itself, as illustrated in Figure 1. To achieve this, we introduce a multi-modal motion representation that decomposes absolute coordinates into joint, bone, and motion streams, thereby providing a superior foundation for both understanding and synthesis. We then build motion generator upon a Coordinates-based Autoregressive Motion Diffusion (CoAMD), which iteratively synthesizes motion in a coarse-to-fine manner. The MAR is trained with dual objectives of fine-grained retrieval and high-level classification. During the autoregressive generation, at each step, we use the MAR to compute a semantic alignment score for the partially generated motion. The gradient of this score is then used to steer the sampling trajectory of the diffusion model, correcting the motion in real-time to better align with the textual semantics. This tight integration of recognition and generation allows our model to produce motions of exceptional fidelity and semantic accuracy.

Our main contributions can be summarized as follows:

- We introduce a unified framework that integrates human motion generation with skeleton-based action recognition, establishing a bidirectional connection between human motion and language semantics.
- We propose Coordinates-based Autoregressive Motion Diffusion (CoAMD), utilizing skeleton coordinates for motion generation while designing a multi-modal action recognizer to provide gradient-based guidance to the motion diffusion model.
- Our method achieves state-of-the-art performance on benchmarks for skeleton-based action recognition, text-to-motion generation, motion editing, and motion–text retrieval, demonstrating both its effectiveness and versatility.

2 Related Work

2.1 Skeleton-Based Action Recognition

Skeleton-based action recognition aims to understand and classify human actions by modeling the dynamics of body joints over time, which are typically represented by absolute coordinates in 3D space (Duan et al., 2022b; Lee et al., 2023; Liu et al., 2025; Wang et al., 2025a). The field evolves rapidly, with state-of-the-art methods largely centering around two prominent architectures: Graph Convolutional Networks (GCNs) and Transformers. GCN-based approaches gain widespread attention due to the natural graph structure of skeleton data, where joints as nodes and bones as edges. The pioneering work of ST-GCN (Yan et al., 2018) first applies graph convolutions to effectively capture the spatio-temporal features of the human skeleton, which spurs a significant amount of follow-up research in this direction (Chi et al., 2022; Duan et al., 2022a; Huang et al., 2023; Zhou et al., 2024b; Xie et al., 2025). In parallel, Transformer-based approaches enter the field for their exceptional ability to model long-range dependencies within sequences (Xin et al., 2023; Wang & Koniusz, 2023; Wu et al., 2024; Do & Kim, 2024), a crucial aspect for understanding complex, long-term actions. With the growing demand for recognizing unseen actions, research focus increasingly shifts towards Zero-Shot Action Recognition (ZSAR) (Zhou et al., 2023; Kuang et al., 2025; Wu et al., 2025c; Zhu et al., 2025; Chen et al., 2025), which aims to classify action categories by aligning visual and semantic spaces. We build upon the transformer-based paradigm for action recognition and adopt a multi-modal approach to capture complex, long-term actions. By leveraging contrastive learning to align visual and semantic spaces, our method supports open-set recognition tasks and further guides the diffusion model to achieve more effective motion generation.

2.2 Text-to-Motion Generation

Text-to-motion generation aims to synthesize realistic human motion from natural language descriptions. Some research adopts VQ-based autoregressive approaches, which discretize continuous motion into a sequence of tokens and employ autoregressive models for generation (Guo et al., 2022b; Zhang et al., 2023a; Yuan et al., 2024; Pinyoanuntapong et al., 2024b; Guo et al., 2024; Pinyoanuntapong et al., 2024a; Lu et al., 2025). Meanwhile, diffusion models emerge as a dominant paradigm for motion generation, inspired by their success in image synthesis Kim et al. (2023); Chen et al. (2023); Yuan et al. (2023); Zhou et al. (2024a); Zhang et al. (2025); Tevet et al. (2025); Zhao et al. (2025). Pioneering works such as MDM and MotionDiffuse demonstrate that learning to progressively denoise a Gaussian distribution under the guidance of text conditions produces diverse and high-quality motions (Tevet et al., 2023; Zhang et al., 2024a). A cornerstone of modern text-to-motion generation is the HumanML3D representation (Guo et al., 2022a). By encoding motion using relative coordinates and incorporating built-in redundant features like local velocities and relative rotations, it significantly simplifies the learning task and becomes the mainstream choice for subsequent methods. Later, the MARDM analyzes and simplifies these redundant features to better suit diffusion models (Meng et al., 2025b). Recently, ACMDM challenges this paradigm by achieving state-of-the-art results using simple absolute joint coordinates (Meng et al., 2025a). Building on these insights, our work adopts absolute coordinates but advances this representation through a multi-modal perspective within the diffusion-based autoregressive framework. We argue that this decomposed, multi-modal representation of absolute coordinates not only facilitates the generation of higher-fidelity motion but also builds a natural bridge to the task of action recognition.

2.3 Unified Human Motion Generation and Understanding

Instead of studying them separately, recent works aim to unify human motion generation and understanding. LaMP (Li et al., 2025b) introduces a language–motion pretraining framework, improving alignment for text-to-motion generation, motion–text retrieval, and motion captioning. KinMo (Zhang et al., 2024b) decomposes motion into joint-group movements and interactions, using a hierarchical semantics and coarse-to-fine synthesis to enable fine-grained text-to-motion retrieval, generation and precise joint control. MG-MotionLLM (Wu et al., 2025a) handles fine-grained motion generation with understanding across multiple temporal granularities. UniMotion (Li et al., 2025a) jointly supports flexible motion control and frame-level motion understanding. Lyu et al. (2025) introduce a lexicalized, sparse motion–language representation to produce interpretable motion descriptors and improve cross-modal alignment. Motion-Agent (Wu et al., 2025b) encodes motions into discrete tokens aligned with LLM vocabularies and enables multi-turn interactive generation. However, these works treat motion understanding merely as motion–text retrieval and motion captioning, and no existing study has yet bridged skeleton-based human action recognition with motion generation, a gap our work seeks to fill.

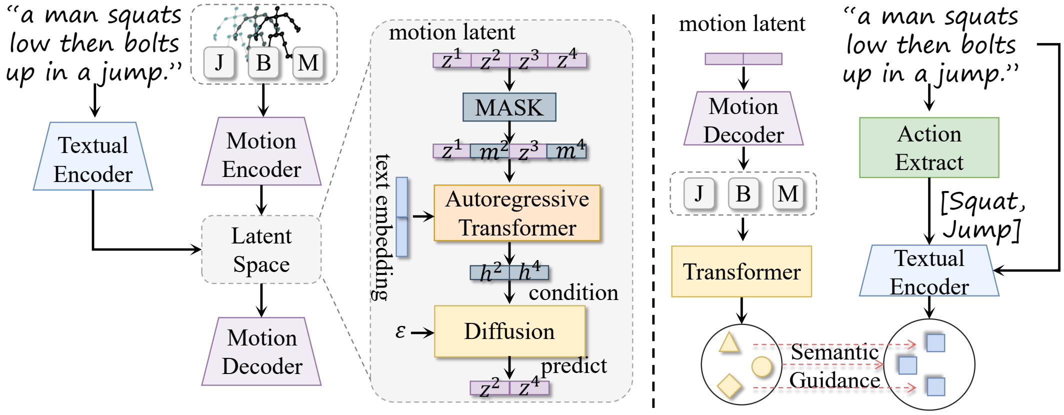

(a) Coordinates-Based Autoregressive Motion Diffusion (b) Semantic Guidance During Sampling

Figure 2: An overview of the CoAMD architecture. (a) The main generative model, which uses a Motion Encoder-Decoder (AE) to map multi-modal inputs into a latent space. A Masked Autoregressive Transformer then processes this latent sequence, with a Diffusion model responsible for filling in the masked tokens. (b) The semantic guidance mechanism during sampling. The MAR computes a semantic alignment score from the decoded motion, and the gradient of this score is used to refine the latent prediction from the diffusion model, ensuring better alignment with the text.

3 Methodology

Our goal is to develop a unified human modeling framework that not only produces controllable and semantically accurate motions but also enables a deeper understanding of the action semantics of human motion. To this end, we propose a novel framework that synergizes a multi-modal action recognizer, a coordinates-based autoregressive motion diffusion, and a semantic mechanism, with an overview of the architecture depicted in Figure 2.

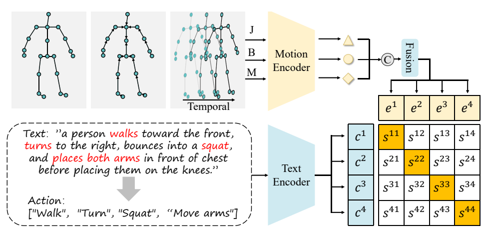

Figure 3: The architecture of our Multi-modal Action Recognizer (MAR), trained with a unified contrastive loss to align embeddings and assess both fine-grained and high-level semantic similarity.

3.1 Multi-modal Action Recognizer

The Multi-modal Action Recognizer (MAR), whose architecture is detailed in Figure 3, is a model trained to comprehend action semantics from two complementary perspectives: fine-grained retrieval and high-level recognition. To facilitate this, we first establish multi-label action classification benchmarks on the HumanML3D and KIT-ML datasets. We process the original annotations by using an LLM to extract core action verbs, followed by applying a balanced K-Means clustering algorithm. This consolidates semantically redundant tags (e.g., "walk", "walks", "walking") into a coherent set of action classes.

The MAR model, R_ϕ, takes our multi-modal motion representation $(\mathbf{X_j}, \mathbf{X_b}, \mathbf{X_m})$ as input and is optimized to produce semantically rich embeddings. The training is driven by a unified contrastive learning objective. Given a batch of N motion-text pairs, we construct sets of motion embeddings $\{\mathbf{e}_i\}_{i=1}^N$ and corresponding text embeddings $\{\mathbf{c}_i\}_{i=1}^N$. The motion embedding set $\mathbf{e}$ includes both the fused representation and the individual modality representations $(\mathbf{e_f}, \mathbf{e_j}, \mathbf{e_b}, \mathbf{e_m})$, while the text embedding set $\mathbf{c}$ includes embeddings for both fine-grained descriptions and high-level action class labels. The model is trained by minimizing the InfoNCE loss across these pairs:

$$\mathcal{L}_{\text{MAR}} = -\frac{1}{N}\sum_{i=1}^{N} \log \frac{\exp(\text{sim}(\mathbf{e}_i, \mathbf{c}_i)/\tau)}{\sum_{k=1}^{N} \exp(\text{sim}(\mathbf{e}_i, \mathbf{c}_k)/\tau)}, \tag{1}$$

where $\text{sim}(\cdot, \cdot)$ denotes cosine similarity and τ is a temperature hyperparameter.

3.2 Coordinates-Based Autoregressive Motion Diffusion

Multi-Modal Motion Representation. Building upon the recent success of using absolute coordinates (Meng et al., 2025a), we introduce a richer, more structured multi-modal motion representation to provide a superior foundation for our model. A given motion sequence, represented by absolute joint coordinates $\mathbf{X_j} \in \mathbb{R}^{L \times J \times 3}$, is decomposed into three complementary streams: the original joints ($\mathbf{X_j}$), bone vectors ($\mathbf{X_b}$), and motion dynamics ($\mathbf{X_m}$). The bone stream, $\mathbf{X_b}$, explicitly models the body's kinematic structure by computing the difference between connected joints. The motion stream, $\mathbf{X_m}$, captures temporal dynamics by calculating the frame-to-frame joint displacement.

These three streams are processed by a Multi-Modal Autoencoder (AE). The AE features shallow, independent projection layers for each modality, followed by an early fusion step and a shared deep encoder $\mathcal{E}$. This maps the multi-modal input to a compact latent representation $\mathbf{z} = \mathcal{E}(\mathbf{X_j}, \mathbf{X_b}, \mathbf{X_m}) \in \mathbb{R}^{L' \times D}$, where L' is the downsampled length and D is the latent dimension. The AE is trained with a multi-modal reconstruction loss. Given the decoded joint sequence $\hat{\mathbf{X}}_\mathbf{j} = \mathcal{D}(\mathbf{z})$, we re-derive the corresponding bone $\hat{\mathbf{X}}_\mathbf{b}$ and motion $\hat{\mathbf{X}}_\mathbf{m}$ streams. The total loss is the sum of the Smooth L1 losses for each stream:

$$\mathcal{L}_{\text{AE}} = \sum_{k \in \{j,b,m\}} \|\mathbf{X}_k - \hat{\mathbf{X}}_k\|_1, \tag{2}$$

The latent representation $\mathbf{z}$ generated under multi-loss constraints exhibits both richness and stability, providing a critical foundation for constructing this diffusion model.

Autoregressive Human Motion Model. We adopt the masked autoregressive generation framework (Li et al., 2024a), which has proven highly effective for motion synthesis. This approach simplifies the generation of a full latent sequence $\mathbf{z} \in \mathbb{R}^{L' \times D}$ by iteratively predicting a randomly masked subset of its tokens, conditioned on the unmasked remainder and a text prompt c. The architecture consists of two core components: a Masked Autoregressive Transformer $\mathcal{T}$ and a Diffusion Model v_θ. First, the latent sequence $\mathbf{z}$ is partitioned into unmasked tokens $\mathbf{z}_{\text{um}}$ and masked tokens $\mathbf{z}_{\text{m}}$. The MAR-Transformer $\mathcal{T}$ processes the unmasked sequence $\mathbf{z}_{\text{um}}$ to produce a contextual embedding $\mathbf{h}$ specifically for the masked positions:

$$\mathbf{h} = \mathcal{T}(\mathbf{z}_{\text{um}}, c). \tag{3}$$

This context $\mathbf{h}$ encapsulates all necessary information from the visible parts of the sequence and the text prompt to guide the generation of the missing parts. Next, the generative step for the masked tokens $\mathbf{z}_{\text{m}}$ is handled by the diffusion model v_θ, which operates on these tokens exclusively. We employ a velocity prediction objective within a flow-matching formulation. The forward process defines a noisy version of the clean masked tokens $\mathbf{z}_{\text{m},0}$ at a continuous timestep $t \in [0, 1)$:

$$\mathbf{z}_{\text{m},t} = (1-t)\mathbf{z}_{\text{m},0} + t\boldsymbol{\epsilon}, \quad \boldsymbol{\epsilon} \sim \mathcal{N}(0, \mathbf{I}). \tag{4}$$

The diffusion model v_θ is then trained to predict the velocity required to denoise $\mathbf{z}_{\text{m},t}$, crucially conditioned on the context $\mathbf{h}$ provided by the transformer. The model is optimized by minimizing the difference between its predicted velocity and the ground-truth velocity derived from the clean target tokens $\mathbf{z}_{\text{m},0}$ and the noise $\boldsymbol{\epsilon}$:

$$\mathcal{L}_{\text{diff}} = \mathbb{E}_{\mathbf{z}_{\text{m},0}, \boldsymbol{\epsilon}, t, \mathbf{h}} \|\mathbf{v}_\theta(\mathbf{z}_{\text{m},t}, t, \mathbf{h}) - (\mathbf{z}_{\text{m},0} - \boldsymbol{\epsilon})\|^2. \tag{5}$$

During inference, for each generative step, we first compute the context $\mathbf{h}$ from the currently unmasked tokens, and then use an ODE solver with the learned velocity field v_θ to sample and fill in the masked tokens.

3.3 Semantic Guidance During Sampling

During the masked autoregressive inference, at each generative step, we leverage the MAR to guide the sampling process. Let $\mathbf{z}$ be the current latent sequence, which contains both previously generated tokens and masked tokens to be filled. The diffusion model first predicts a preliminary update for the masked tokens, resulting in a complete latent sequence $\mathbf{z}'$. We then compute a guidance gradient to refine this prediction.

First, the complete latent sequence $\mathbf{z}'$ is decoded into an estimated motion $\hat{\mathbf{X}} = \mathcal{D}(\mathbf{z}')$. Then, a composite semantic alignment score $\mathcal{S}$ is calculated. This score is based on the alignment of the fused and modality-specific embeddings with the target text embedding c:

$$\mathcal{S}(\hat{\mathbf{X}}, c) = \sum_{k \in \{f,j,b,m\}} w_k \cdot \mathrm{sim}(R_\phi^k(\hat{\mathbf{X}}), c), \tag{6}$$

where R_ϕ^k denotes the specific embedding from the MAR (with f for fused) and w_k are weighting coefficients. With this score, we compute its gradient with respect to the latent sequence $\mathbf{z}'$. To ensure stable updates, the gradient is normalized:

$$\mathbf{g} = \nabla_{\mathbf{z}'} \mathcal{S}(\mathcal{D}(\mathbf{z}'), c), \quad \hat{\mathbf{g}} = \frac{\mathbf{g}}{\|\mathbf{g}\|_2 + \epsilon}. \tag{7}$$

This normalized gradient $\hat{\mathbf{g}}$ points in the direction of steepest ascent for the text-motion alignment score. The final updated latent sequence $\mathbf{z}_{\text{new}}$ is obtained by applying this gradient step only to the tokens that are masked in the current iteration (M_t):

$$\mathbf{z}_{\text{new}} = \mathbf{z}' + \gamma \cdot \hat{\mathbf{g}} \odot M_t, \tag{8}$$

where γ is a guidance scale hyperparameter and $\odot$ denotes element-wise multiplication. By incorporating this gradient-based guidance step within each iteration of the autoregressive process, we actively steer the generation towards states that are not only probable under the diffusion model but also highly aligned with the detailed semantics of the text prompt.

4 Experiments

4.1 Datasets and Evaluation Protocols

Action Recognition. To construct the reward model, we establish multi-label classification benchmarks on both HumanML3D (Guo et al., 2022a) by processing and clustering their annotations into 400 classes, respectively. Our analysis reveals a significant long-tail distribution within these classes, where a minority of "head" classes contain the majority of samples. To systematically assess performance under this imbalance, we partition the classes into three frequency-based subsets: Head (top 10%), Medium (next 30%), and Tail (bottom 60%). Furthermore, to evaluate the cross-dataset generalization of our recognizer, we also test its performance on the widely-used NTU-RGB+D 60 (Shahroudy et al., 2016) and NTU-RGB+D 120 (Liu et al., 2019) benchmarks.

Motion Generation. We validate our approach on two standard text-to-motion benchmarks: HumanML3D and KIT-ML. Consistent with the state-of-the-art paradigm, all models are trained and evaluated using absolute joint coordinates. To ensure a fair and comprehensive comparison, we adopt the robust evaluation framework from (Meng et al., 2025a). Our quantitative assessment relies on a suite of standard metrics: R-Precision (Top-1/2/3) to measure text-motion matching accuracy; Fréchet Inception Distance (FID) and MM-Dist to evaluate distributional similarity to real motions; Multi-Modality to quantify the diversity of generated samples per prompt; and CLIP Score to assess the fine-grained alignment via cosine similarity in a shared embedding space.

4.2 Main Results

Text-to-Motion Generation. Table 1 and Table 2 present a quantitative comparison of our method CoAMD against state-of-the-art baselines on the HumanML3D and KIT datasets. Our unguided model (CoAMD w/o MAR), which leverages the proposed multi-modal representation and already demonstrates highly competitive results outperforming most existing methods. This validates the effectiveness of our foundational architecture. When augmented with our Multi-modal Action Recognizer for guidance (CoAMD (ours)), the model's performance is substantially boosted, setting new state-of-the-art scores across nearly all metrics on both benchmarks. The notable improvements in FID and CLIP-Score highlight our guidance mechanism's dual benefit. It enhances the distributional realism of generated motions and simultaneously improves the fine-grained semantic alignment with input text prompts. This demonstrates that integrating an explicit action understanding module into the generative process is a highly effective strategy for advancing text-to-motion synthesis.

Table 1: Evaluation of text-to-motion generation performance on the HumanML3D dataset.

Methods	R-Precision↑			FID↓	MM-Dist↓	MModality↑	CLIP-score↑
	Top 1	Top 2	Top 3				
MDM (2023)	$0.440^{\pm.007}$	$0.636^{\pm.006}$	$0.742^{\pm.006}$	$0.518^{\pm.032}$	$3.640^{\pm.023}$	$3.604^{\pm.031}$	$0.578^{\pm.003}$
MotionDiffuse (2024a)	$0.467^{\pm.006}$	$0.641^{\pm.005}$	$0.753^{\pm.005}$	$0.778^{\pm.005}$	$3.490^{\pm.023}$	$3.179^{\pm.046}$	$0.606^{\pm.004}$
ReMoDiffuse (2023b)	$0.468^{\pm.003}$	$0.653^{\pm.003}$	$0.754^{\pm.005}$	$0.883^{\pm.021}$	$3.414^{\pm.022}$	$3.703^{\pm.154}$	$0.621^{\pm.003}$
MLD++ (2024)	$0.501^{\pm.004}$	$0.682^{\pm.004}$	$0.789^{\pm.003}$	$2.027^{\pm.021}$	$3.220^{\pm.021}$	$1.924^{\pm.065}$	$0.637^{\pm.003}$
MotionLCM V2 (2024)	$0.501^{\pm.002}$	$0.693^{\pm.002}$	$0.790^{\pm.002}$	$2.267^{\pm.023}$	$3.192^{\pm.062}$	$1.780^{\pm.062}$	$0.640^{\pm.003}$
MARDM-ϵ (2025b)	$0.492^{\pm.006}$	$0.696^{\pm.005}$	$0.793^{\pm.003}$	$0.116^{\pm.002}$	$3.349^{\pm.010}$	$2.470^{\pm.053}$	$0.635^{\pm.003}$
MARDM-v (2025b)	$0.499^{\pm.005}$	$0.696^{\pm.005}$	$0.795^{\pm.003}$	$0.114^{\pm.007}$	$3.270^{\pm.009}$	$2.377^{\pm.062}$	$0.637^{\pm.002}$
ACMDM-S-PS22 (2025a)	$0.508^{\pm.002}$	$0.701^{\pm.003}$	$0.798^{\pm.003}$	$0.109^{\pm.005}$	$3.253^{\pm.008}$	$2.156^{\pm.061}$	$0.642^{\pm.001}$
CoAMD w/o MAR	$0.512^{\pm.002}$	$0.705^{\pm.002}$	$0.801^{\pm.002}$	$0.074^{\pm.004}$	$2.980^{\pm.008}$	$2.012^{\pm.034}$	$0.668^{\pm.001}$
CoAMD (ours)	$0.519^{\pm.003}$	$0.708^{\pm.002}$	$0.803^{\pm.002}$	$0.065^{\pm.004}$	$2.959^{\pm.009}$	$2.014^{\pm.036}$	$0.674^{\pm.002}$

Table 2: Evaluation of text-to-motion generation performance on the KIT dataset.

Methods	R-Precision↑			FID↓	MM-Dist↓	MModality↑	CLIP-score↑
	Top 1	Top 2	Top 3				
MDM (2023)	$0.333^{\pm.012}$	$0.561^{\pm.009}$	$0.689^{\pm.009}$	$0.585^{\pm.043}$	$4.002^{\pm.033}$	$1.681^{\pm.107}$	$0.605^{\pm.007}$
MotionDiffuse (2024a)	$0.344^{\pm.009}$	$0.536^{\pm.007}$	$0.658^{\pm.007}$	$3.845^{\pm.087}$	$4.167^{\pm.054}$	$1.774^{\pm.217}$	$0.626^{\pm.006}$
ReMoDiffuse (2023b)	$0.356^{\pm.004}$	$0.572^{\pm.007}$	$0.706^{\pm.009}$	$1.725^{\pm.053}$	$3.735^{\pm.036}$	$1.928^{\pm.127}$	$0.665^{\pm.005}$
MARDM-ϵ (2025b)	$0.375^{\pm.006}$	$0.597^{\pm.008}$	$0.739^{\pm.006}$	$0.340^{\pm.020}$	$3.489^{\pm.018}$	$1.479^{\pm.078}$	$0.681^{\pm.003}$
MARDM-v (2025b)	$0.387^{\pm.006}$	$0.610^{\pm.006}$	$0.749^{\pm.006}$	$0.242^{\pm.014}$	$3.374^{\pm.019}$	$1.312^{\pm.053}$	$0.692^{\pm.002}$
ACMDM-S-PS22 (2025a)	$0.391^{\pm.005}$	$0.615^{\pm.005}$	$0.752^{\pm.006}$	$0.237^{\pm.010}$	$3.368^{\pm.019}$	$1.267^{\pm.063}$	$0.696^{\pm.002}$
CoAMD (ours)	$0.431^{\pm.005}$	$0.659^{\pm.007}$	$0.785^{\pm.006}$	$0.217^{\pm.009}$	$2.966^{\pm.019}$	$1.383^{\pm.067}$	$0.708^{\pm.002}$

Table 3: Comparison of action recognition performance on the HumanML3D dataset.

Method	Modality	HumanML3D(%)			
		Overall	Many-shot	Medium-shot	Few-shot
CADA-VAE (Schonfeld et al., 2019)	J	43.62	55.97	28.54	12.32
SMIE (Zhou et al., 2023)	J	49.23	60.44	36.57	23.61
DVTA (Kuang et al., 2025)	J	50.05	61.12	37.24	24.52
CoAMD (ours)	J	49.11	60.13	36.14	22.91
CoAMD (ours)	J+B+M	51.63	62.24	38.13	25.32

Skeleton-Based Action Recognition. Since our framework synergizes motion generation and action recognition, we evaluate the effectiveness of the MAR, which provides semantic guidance signals. Using absolute joint coordinates as the foundation of our representation naturally suits the action recognition task. As described in Section 3.1, we establish new action recognition benchmarks on the HumanML3D dataset originally designed for synthesis. Table 3 compares our method against alignment-based action recognition baselines. To ensure fairness, all baseline methods are re-implemented to employ the same visual backbone as our model. The results clearly demonstrate the superiority of our approach. When multi-modal representations are employed (J+B+M), the performance is further and significantly improved. Notably, the most substantial gains are observed in the few-shot classes of both datasets. This strongly supports that explicitly modeling body kinematics (bones) and temporal dynamics (motion) provides richer and more discriminative features. These results validate MAR as a reliable source of semantic guidance for our generation task.

Table 4: Cross-dataset generalization performance on NTU-60 and NTU-120. Our model is pre-trained on HumanML3D and evaluated using a linear probing protocol.

Method	Modality	NTU-60		NTU-120	
		x-sub	x-view	x-sub	x-set
UmURL (Sun et al., 2023)	J	42.31	44.98	32.14	33.81
USDRL (Wang et al., 2025a)	J	43.48	46.23	33.02	34.69
CoAMD (ours)	J	45.12	48.29	34.41	36.09
UmURL (Sun et al., 2023)	J+B+M	47.11	50.62	36.19	37.59
USDRL (Wang et al., 2025a)	J+B+M	48.02	52.08	37.01	37.98
CoAMD (ours)	J+B+M	50.24	54.04	38.29	39.11

Cross-Dataset Generalization. To assess the robustness and transferability of the features learned by our MAR, we evaluate its cross-dataset generalization capability on the NTU-60 and NTU-120 benchmarks. Our MAR is pre-trained solely on the text-motion alignment task of HumanML3D. Following a standard linear probing protocol, we freeze the MAR backbone and train only a linear classification head on the target NTU datasets. To handle heterogeneous skeletons, we map the joints from NTU to their corresponding locations in our model's topology. As shown in Table 4, our full multi-modal model consistently outperforms baselines across every setting. This performance is noteworthy as the features are learned without exposure to the target datasets or their labels. It validates that our representation captures a transferable understanding of human motion semantics, robust to generalize to new datasets with different skeletal structures and action vocabularies.

Table 5: Performance comparison on text-motion and motion-text retrieval tasks on the HumanML3D dataset.

Methods	Text-Motion(%)					Motion-Text(%)				
	R@1	R@2	R@3	R@5	R@10	R@1	R@2	R@3	R@5	R@10
TEMOS (Petrovich et al., 2022)	40.49	53.52	61.14	70.96	84.15	39.96	53.49	61.79	72.40	85.89
T2M (Guo et al., 2022a)	52.48	71.05	80.65	89.66	96.58	52.00	71.21	81.11	89.87	96.78
TMR (Petrovich et al., 2023)	67.16	81.32	86.81	91.43	95.36	67.97	81.20	86.35	91.70	95.27
LaMP (Li et al., 2024b)	67.18	81.90	87.04	92.00	95.73	68.02	82.10	87.50	92.20	96.90
CoAMD (ours)	68.33	82.61	88.05	92.45	95.97	68.86	82.77	88.09	92.36	97.21

Text-Motion Retrieval. Beyond its primary role as a source of semantic guidance for generation, the MAR is an inherently powerful text-motion alignment model capable of cross-modal retrieval. To validate this capability, we evaluate its performance on both text-to-motion and motion-to-text retrieval using the HumanML3D benchmark. As shown in Table 5, we compare our MAR against several state-of-the-art methods designed specifically for motion retrieval. The evaluation is conducted using a standard batch size of 32 for a fair comparison. Our model demonstrates superior performance, achieving the highest scores across nearly all settings. This retrieval capability is a direct result of our dual-task pre-training objective, which forces the model to learn a fine-grained, shared embedding space where motion and text are tightly aligned. This result showcases the versatility of our MAR and provides further evidence for its suitability as a high-quality guidance source.

Motion Editing. A key strength of our masked autoregressive framework is its ability to handle motion editing tasks without task-specific modifications. We evaluate on HumanML3D under four

Table 6: Quantitative comparison on temporal editing tasks on the HumanML3D dataset.

Tasks	Methods	R-Precision↑			FID↓	MM-Dist↓	CLIP-score↑
		Top 1	Top 2	Top 3			
Temporal Inpainting	BAMM (Pinyoanuntapong et al., 2024a)	0.387	0.554	0.649	0.385	4.046	0.574
	MARDM (2025b)	0.503	0.702	0.795	0.120	3.051	0.671
	CoAMD (ours)	0.518	0.716	0.804	0.023	2.943	0.677
Temporal Outpainting	BAMM (Pinyoanuntapong et al., 2024a)	0.433	0.605	0.707	0.206	3.615	0.613
	MARDM (Meng et al., 2025b)	0.512	0.705	0.797	0.114	3.065	0.671
	CoAMD (ours)	0.518	0.703	0.800	0.022	2.967	0.675
Prefix	BAMM (Pinyoanuntapong et al., 2024a)	0.352	0.526	0.632	0.578	4.178	0.565
	MARDM (Meng et al., 2025b)	0.515	0.709	0.800	0.120	3.039	0.673
	CoAMD (ours)	0.525	0.707	0.802	0.032	2.934	0.679
Suffix	BAMM (Pinyoanuntapong et al., 2024a)	0.435	0.608	0.708	0.201	3.504	0.625
	MARDM (Meng et al., 2025b)	0.501	0.685	0.780	0.138	3.113	0.668
	CoAMD (ours)	0.522	0.705	0.804	0.039	3.000	0.674

standard benchmarks: Temporal Inpainting Temporal Outpainting Prefix and Suffix generation. As shown in Table 6, our method outperforms strong baselines across all settings. It achieves higher R-Precision indicating better semantic alignment. It also obtains lower FID and MM-Dist showing improved realism and faithfulness to the ground truth. These results confirm our multi-modal representation and semantic guidance provide a stronger conditioning signal for controllable synthesis.

Table 7: Impact of different modality combinations on the HumanML3D dataset. Progressively adding Bone (B) and Motion (M) modalities to the baseline Joint (J) representation improves performance on both generation (R-Precision, FID, MM-Dist, CLIP-score) and recognition (Accuracy) tasks.

Modality	R-Precision↑			FID↓	MM-Dist↓	CLIP-score↑	Top-1 Accuracy(%)			
	Top 1	Top 2	Top 3				Overall	Many-shot	Medium-shot	Few-shot
J	0.512	0.705	0.801	0.074	2.980	0.668	49.11	60.13	36.14	22.91
J+B	0.515	0.706	0.802	0.072	2.975	0.670	49.85	61.02	37.00	23.65
J+M	0.517	0.707	0.803	0.069	2.970	0.672	50.22	61.53	37.52	24.10
J+B+M	0.519	0.708	0.803	0.065	2.959	0.674	51.63	62.24	38.13	25.32

4.3 Ablation Study

Effectiveness of Multi-Modal Representation. We first investigate the impact of our multi-modal representation on both generation and recognition. As detailed in Table 7, we progressively integrate the bone (B) and motion (M) modalities with the baseline joint (J) representation. The results clearly indicate that enriching the representation yields consistent improvements across both tasks. For motion generation, incorporating more modalities enhances the quality of the learned latent space, leading to a steady decrease in the FID score and signifying more realistic motions. For recognition, the additional modalities provide richer features, boosting the MAR's capability and increasing the Overall Top-1 Accuracy. This enhanced recognition power provides a more precise guidance signal, raising the R-Precision. This synergistic relationship validates our hypothesis that a unified, multi-modal representation is mutually beneficial for understanding and synthesizing human motion.

Table 8: Ablation study on the MAR semantic guidance mechanism and its integration with the autoregressive process.

method	R-Precision↑			FID↓	MM-Dist↓	MModality↑	CLIP-score↑
	Top 1	Top 2	Top 3				
w/ MAR(J+B+M)	0.519	0.708	0.803	0.065	2.959	2.014	0.674
w/ MAR(J)	0.514	0.707	0.796	0.095	2.984	2.192	0.672
w/o MAR	0.512	0.705	0.801	0.074	2.980	2.012	0.668
w/o Autoregression	0.488	0.685	0.781	0.142	3.125	2.421	0.663

Effectiveness Semantic Guidance for Motion Generation. Table 8 presents an ablation on our core contribution of iterative semantic guidance. The unguided baseline (w/o MAR) exhibits the lowest overall text-alignment scores. Introducing guidance from the MAR (w/ MAR(J+B+M)) substantially improves performance, reducing FID by nearly 50% and boosting R-Precision, which confirms the efficacy of the guidance signal itself. Critically, to isolate the importance of the iterative application, we test a non-autoregressive variant (w/o Autoregression) where guidance is applied only once. This model's performance falls below the unguided baseline. It demonstrates that a single corrective signal applied to a flawed final output is ineffective. In contrast, our method's step-by-step guidance enables continuous, fine-grained refinements throughout the autoregressive process. This iterative steering prevents the accumulation of semantic errors, validating that the key contribution arises from the tight integration of semantic guidance with the iterative sampling process.

5 CONCLUSION

In this work, we introduce CoAMD, a unified framework that integrates text-to-motion generation with skeleton-based action recognition. We show that replacing separate training paradigms with an integrated design, where a strong action recognizer serves as an active semantic guide, yields substantial improvements in both motion quality and text alignment. A central insight is that iterative integration of guidance throughout the masked autoregressive sampling process is essential, as it enables continuous and fine-grained corrections that outperform single post-hoc refinements. Moreover, our multi-modal representation proves mutually beneficial, enriching feature diversity to enhance both generative fidelity and recognition robustness.

Limitations and Future Work. We recognize certain limitations in our approach and highlight promising directions for future work. Our framework currently focuses on text-driven single-person motion. Extending it to multi-agent or multimodal scenarios is a promising direction. Moreover, while iterative guidance improves semantic precision, it incurs inference overhead. Exploring efficient alternatives, such as distillation into the generator, could balance accuracy and speed.

ETHICS STATEMENT

This work studies motion generation and understanding, which has wide applications in virtual avatars, animation, human-computer interaction, and robotics. We recognize potential ethical risks, including the misuse of generated motions for creating deceptive content or impersonating individuals. Our research is intended purely for academic purposes. All experiments are conducted on publicly available datasets that do not contain personally identifiable or sensitive information. We encourage responsible use of such technologies with appropriate safeguards to mitigate malicious applications.

REPRODUCIBILITY STATEMENT

We provide all necessary details to reproduce our experiments, including model architectures, training settings and hyperparameters. Our code and pre-trained models will be released to facilitate reproducibility.

REFERENCES

Xin Chen, Biao Jiang, Wen Liu, Zilong Huang, Bin Fu, Tao Chen, and Gang Yu. Executing your commands via motion diffusion in latent space. In *Proceedings of the IEEE/CVF Conference on Computer Vision and Pattern Recognition*, pp. 18000–18010, 2023.

Yang Chen, Jingcai Guo, Song Guo, and Dacheng Tao. Neuron: Learning context-aware evolving representations for zero-shot skeleton action recognition. In *Proceedings of the Computer Vision and Pattern Recognition Conference*, pp. 8721–8730, 2025.

Hyung-gun Chi, Myoung Hoon Ha, Seunggeun Chi, Sang Wan Lee, Qixing Huang, and Karthik Ramani. Infogcn: Representation learning for human skeleton-based action recognition. In *Proceedings of the IEEE/CVF Conference on Computer Vision and Pattern Recognition*, pp. 20186–20196, 2022.

Wenxun Dai, Ling-Hao Chen, Jingbo Wang, Jinpeng Liu, Bo Dai, and Yansong Tang. Motionlcm: Real-time controllable motion generation via latent consistency model. In *European Conference on Computer Vision*, pp. 390–408. Springer, 2024.

Jeonghyeok Do and Munchurl Kim. Skateformer: skeletal-temporal transformer for human action recognition. In *European Conference on Computer Vision*, pp. 401–420. Springer, 2024.

Yong Du, Wei Wang, and Liang Wang. Hierarchical recurrent neural network for skeleton based action recognition. In *Proceedings of the IEEE Conference on Computer Vision and Pattern Recognition*, pp. 1110–1118, 2015.

Haodong Duan, Jiaqi Wang, Kai Chen, and Dahua Lin. Pyskl: Towards good practices for skeleton action recognition. In *Proceedings of the 30th ACM international conference on multimedia*, pp. 7351–7354, 2022a.

Haodong Duan, Yue Zhao, Kai Chen, Dahua Lin, and Bo Dai. Revisiting skeleton-based action recognition. In *Proceedings of the IEEE/CVF Conference on Computer Vision and Pattern Recognition*, pp. 2969–2978, 2022b.

Chuan Guo, Shihao Zou, Xinxin Zuo, Sen Wang, Wei Ji, Xingyu Li, and Li Cheng. Generating diverse and natural 3d human motions from text. In *Proceedings of the IEEE/CVF Conference on Computer Vision and Pattern Recognition*, pp. 5152–5161, 2022a.

Chuan Guo, Xinxin Zuo, Sen Wang, and Li Cheng. Tm2t: Stochastic and tokenized modeling for the reciprocal generation of 3d human motions and texts. In *European Conference on Computer Vision*, pp. 580–597. Springer, 2022b.

Chuan Guo, Yuxuan Mu, Muhammad Gohar Javed, Sen Wang, and Li Cheng. Momask: Generative masked modeling of 3d human motions. In *Proceedings of the IEEE/CVF Conference on Computer Vision and Pattern Recognition*, pp. 1900–1910, 2024.

Xiaohu Huang, Hao Zhou, Jian Wang, Haocheng Feng, Junyu Han, Errui Ding, Jingdong Wang, Xinggang Wang, Wenyu Liu, and Bin Feng. Graph contrastive learning for skeleton-based action recognition. *arXiv preprint arXiv:2301.10900*, 2023.

Biao Jiang, Xin Chen, Wen Liu, Jingyi Yu, Gang Yu, and Tao Chen. Motiongpt: Human motion as a foreign language. *Advances in Neural Information Processing Systems*, 36:20067–20079, 2023.

Jihoon Kim, Jiseob Kim, and Sungjoon Choi. Flame: Free-form language-based motion synthesis & editing. In *Proceedings of the AAAI Conference on Artificial Intelligence*, volume 37, pp. 8255–8263, 2023.

Jidong Kuang, Hongsong Wang, Chaolei Han, Yang Zhang, and Jie Gui. Zero-shot skeleton-based action recognition with dual visual-text alignment. *Pattern Recognition*, pp. 112342, 2025.

Jungho Lee, Minhyeok Lee, Dogyoon Lee, and Sangyoun Lee. Hierarchically decomposed graph convolutional networks for skeleton-based action recognition. In *Proceedings of the IEEE/CVF International Conference on Computer Vision*, pp. 10444–10453, 2023.

Chuqiao Li, Julian Chibane, Yannan He, Naama Pearl, Andreas Geiger, and Gerard Pons-Moll. Unimotion: Unifying 3d human motion synthesis and understanding. In *International Conference on 3D Vision*, pp. 240–249. IEEE, 2025a.

Tianhong Li, Yonglong Tian, He Li, Mingyang Deng, and Kaiming He. Autoregressive image generation without vector quantization. *Advances in Neural Information Processing Systems*, 37: 56424–56445, 2024a.

Zhe Li, Weihao Yuan, Yisheng He, Lingteng Qiu, Shenhao Zhu, Xiaodong Gu, Weichao Shen, Yuan Dong, Zilong Dong, and Laurence T Yang. LaMP: Language-motion pretraining for motion generation, retrieval, and captioning. *arXiv preprint arXiv:2410.07093*, 2024b.

Zhe Li, Weihao Yuan, Lingteng Qiu, Shenhao Zhu, Xiaodong Gu, Weichao Shen, Yuan Dong, Zilong Dong, Laurence Tianruo Yang, et al. Lamp: Language-motion pretraining for motion generation, retrieval, and captioning. In *International Conference on Learning Representations*, 2025b.

Jun Liu, Amir Shahroudy, Mauricio Perez, Gang Wang, Ling-Yu Duan, and Alex C Kot. Ntu rgb+ d 120: A large-scale benchmark for 3d human activity understanding. *IEEE Transactions on Pattern Analysis and Machine Intelligence*, 42(10):2684–2701, 2019.

Mengyuan Liu, Hong Liu, Qianshuo Hu, Bin Ren, Junsong Yuan, Jiaying Lin, and Jiajun Wen. 3d skeleton-based action recognition: A review. *arXiv preprint arXiv:2506.00915*, 2025.

Shunlin Lu, Jingbo Wang, Zeyu Lu, Ling-Hao Chen, Wenxun Dai, Junting Dong, Zhiyang Dou, Bo Dai, and Ruimao Zhang. Scamo: Exploring the scaling law in autoregressive motion generation model. In *Proceedings of the Computer Vision and Pattern Recognition Conference*, pp. 27872–27882, 2025.

Guangtao Lyu, Chenghao Xu, Jiexi Yan, Muli Yang, and Cheng Deng. Towards unified human motion-language understanding via sparse interpretable characterization. In *International Conference on Learning Representations*, 2025.

Zichong Meng, Zeyu Han, Xiaogang Peng, Yiming Xie, and Huaizu Jiang. Absolute coordinates make motion generation easy. *arXiv preprint arXiv:2505.19377*, 2025a.

Zichong Meng, Yiming Xie, Xiaogang Peng, Zeyu Han, and Huaizu Jiang. Rethinking diffusion for text-driven human motion generation: Redundant representations, evaluation, and masked autoregression. In *Proceedings of the Computer Vision and Pattern Recognition Conference*, pp. 27859–27871, 2025b.

Mathis Petrovich, Michael J Black, and Gül Varol. Temos: Generating diverse human motions from textual descriptions. In *European Conference on Computer Vision*, pp. 480–497. Springer, 2022.

Mathis Petrovich, Michael J Black, and Gül Varol. TMR: Text-to-motion retrieval using contrastive 3d human motion synthesis. In *Proceedings of the IEEE/CVF International Conference on Computer Vision*, pp. 9488–9497, 2023.

Ekkasit Pinyoanuntapong, Muhammad Usama Saleem, Pu Wang, Minwoo Lee, Srijan Das, and Chen Chen. BAMM: Bidirectional autoregressive motion model. In *European Conference on Computer Vision*, pp. 172–190. Springer, 2024a.

Ekkasit Pinyoanuntapong, Pu Wang, Minwoo Lee, and Chen Chen. Mmm: Generative masked motion model. In *Proceedings of the IEEE/CVF Conference on Computer Vision and Pattern Recognition*, pp. 1546–1555, 2024b.

Aditya Ramesh, Prafulla Dhariwal, Alex Nichol, Casey Chu, and Mark Chen. Hierarchical text-conditional image generation with clip latents. *arXiv preprint arXiv:2204.06125*, 1(2):3, 2022.

Chitwan Saharia, William Chan, Saurabh Saxena, Lala Li, Jay Whang, Emily L Denton, Kamyar Ghasemipour, Raphael Gontijo Lopes, Burcu Karagol Ayan, Tim Salimans, et al. Photorealistic text-to-image diffusion models with deep language understanding. *Advances in neural information processing systems*, 35:36479–36494, 2022.

Edgar Schonfeld, Sayna Ebrahimi, Samarth Sinha, Trevor Darrell, and Zeynep Akata. Generalized zero-and few-shot learning via aligned variational autoencoders. In *Proceedings of the IEEE/CVF Conference on Computer Vision and Pattern Recognition*, pp. 8247–8255, 2019.

Amir Shahroudy, Jun Liu, Tian-Tsong Ng, and Gang Wang. Ntu rgb+ d: A large scale dataset for 3d human activity analysis. In *Proceedings of the IEEE Conference on Computer Vision and Pattern Recognition*, pp. 1010–1019, 2016.

Shengkai Sun, Daizong Liu, Jianfeng Dong, Xiaoye Qu, Junyu Gao, Xun Yang, Xun Wang, and Meng Wang. Unified multi-modal unsupervised representation learning for skeleton-based action understanding. In *Proceedings of the ACM International Conference on Multimedia*, pp. 2973–2984, 2023.

Shixiang Tang, Yizhou Wang, Lu Chen, Yuan Wang, Sida Peng, Dan Xu, and Wanli Ouyang. Human-centric foundation models: Perception, generation and agentic modeling. In *Proceedings of the International Joint Conference on Artificial Intelligence*, pp. 10678–10686. International Joint Conferences on Artificial Intelligence Organization, 2025. Survey Track.

Guy Tevet, Sigal Raab, Brian Gordon, Yoni Shafir, Daniel Cohen-or, and Amit Haim Bermano. Human motion diffusion model. In *International Conference on Learning Representations*, 2023.

Guy Tevet, Sigal Raab, Setareh Cohan, Daniele Reda, Zhengyi Luo, Xue Bin Peng, Amit Haim Bermano, and Michiel van de Panne. Closd: Closing the loop between simulation and diffusion for multi-task character control. In *International Conference on Learning Representations*, 2025.

Hongsong Wang and Liang Wang. Modeling temporal dynamics and spatial configurations of actions using two-stream recurrent neural networks. In *Proceedings of the IEEE Conference on Computer Vision and Pattern Recognition*, pp. 499–508, 2017.

Hongsong Wang, Wanjiang Weng, Junbo Wang, Fang Zhao, Guo-Sen Xie, Xin Geng, and Liang Wang. Foundation model for skeleton-based human action understanding. *IEEE Transactions on Pattern Analysis and Machine Intelligence*, 2025a.

Lei Wang and Piotr Koniusz. 3mformer: Multi-order multi-mode transformer for skeletal action recognition. In *Proceedings of the IEEE/CVF Conference on Computer Vision and Pattern Recognition*, pp. 5620–5631, 2023.

Yizhou Wang, Yixuan Wu, Weizhen He, Xun Guo, Feng Zhu, Lei Bai, Rui Zhao, Jian Wu, Tong He, Wanli Ouyang, et al. Hulk: A universal knowledge translator for human-centric tasks. *IEEE Transactions on Pattern Analysis and Machine Intelligence*, 2025b.

Bizhu Wu, Jinheng Xie, Keming Shen, Zhe Kong, Jianfeng Ren, Ruibin Bai, Rong Qu, and Linlin Shen. Mg-motionllm: A unified framework for motion comprehension and generation across multiple granularities. In *Proceedings of the Computer Vision and Pattern Recognition Conference*, pp. 27849–27858, 2025a.

Qi Wu, Yubo Zhao, Yifan Wang, Xinhang Liu, Yu-Wing Tai, and Chi-Keung Tang. Motion-agent: A conversational framework for human motion generation with llms. In *International Conference on Learning Representations*, 2025b.

Wenhan Wu, Ce Zheng, Zihao Yang, Chen Chen, Srijan Das, and Aidong Lu. Frequency guidance matters: Skeletal action recognition by frequency-aware mixed transformer. In *Proceedings of the ACM International Conference on Multimedia*, pp. 4660–4669, 2024.

Wenhan Wu, Zhishuai Guo, Chen Chen, Hongfei Xue, and Aidong Lu. Frequency-semantic enhanced variational autoencoder for zero-shot skeleton-based action recognition. *arXiv preprint arXiv:2506.22179*, 2025c.

Jianyang Xie, Yitian Zhao, Yanda Meng, He Zhao, Anh Nguyen, and Yalin Zheng. Are spatial-temporal graph convolution networks for human action recognition over-parameterized? In *Proceedings of the Computer Vision and Pattern Recognition Conference*, pp. 24309–24319, 2025.

Wentian Xin, Qiguang Miao, Yi Liu, Ruyi Liu, Chi-Man Pun, and Cheng Shi. Skeleton mixformer: Multivariate topology representation for skeleton-based action recognition. In *Proceedings of the ACM International Conference on Multimedia*, pp. 2211–2220, 2023.

Sijie Yan, Yuanjun Xiong, and Dahua Lin. Spatial temporal graph convolutional networks for skeleton-based action recognition. In *Proceedings of the AAAI conference on artificial intelligence*, volume 32, 2018.

Weihao Yuan, Yisheng He, Weichao Shen, Yuan Dong, Xiaodong Gu, Zilong Dong, Liefeng Bo, and Qixing Huang. Mogents: Motion generation based on spatial-temporal joint modeling. *Advances in Neural Information Processing Systems*, 37:130739–130763, 2024.

Ye Yuan, Jiaming Song, Umar Iqbal, Arash Vahdat, and Jan Kautz. Physdiff: Physics-guided human motion diffusion model. In *Proceedings of the IEEE/CVF International Conference on Computer Vision*, pp. 16010–16021, 2023.

Jianrong Zhang, Yangsong Zhang, Xiaodong Cun, Yong Zhang, Hongwei Zhao, Hongtao Lu, Xi Shen, and Ying Shan. Generating human motion from textual descriptions with discrete representations. In *Proceedings of the IEEE/CVF Conference on Computer Vision and Pattern Recognition*, pp. 14730–14740, 2023a.

Jianrong Zhang, Hehe Fan, and Yi Yang. Energymogen: Compositional human motion generation with energy-based diffusion model in latent space. In *Proceedings of the Computer Vision and Pattern Recognition Conference*, pp. 17592–17602, 2025.

Mingyuan Zhang, Xinying Guo, Liang Pan, Zhongang Cai, Fangzhou Hong, Huirong Li, Lei Yang, and Ziwei Liu. Remodiffuse: Retrieval-augmented motion diffusion model. In *Proceedings of the IEEE/CVF International Conference on Computer Vision*, pp. 364–373, 2023b.

Mingyuan Zhang, Zhongang Cai, Liang Pan, Fangzhou Hong, Xinying Guo, Lei Yang, and Ziwei Liu. Motiondiffuse: Text-driven human motion generation with diffusion model. *IEEE Transactions on Pattern Analysis and Machine Intelligence*, 46(6):4115–4128, 2024a.

Pengfei Zhang, Pinxin Liu, Pablo Garrido, Hyeongwoo Kim, and Bindita Chaudhuri. Kinmo: Kinematic-aware human motion understanding and generation. *arXiv preprint arXiv:2411.15472*, 2024b.

Kaifeng Zhao, Gen Li, and Siyu Tang. Dartcontrol: A diffusion-based autoregressive motion model for real-time text-driven motion control. In *International Conference on Learning Representations*, 2025.

Wenyang Zhou, Zhiyang Dou, Zeyu Cao, Zhouyingcheng Liao, Jingbo Wang, Wenjia Wang, Yuan Liu, Taku Komura, Wenping Wang, and Lingjie Liu. Emdm: Efficient motion diffusion model for fast and high-quality motion generation. In *European Conference on Computer Vision*, pp. 18–38. Springer, 2024a.

Yujie Zhou, Wenwen Qiang, Anyi Rao, Ning Lin, Bing Su, and Jiaqi Wang. Zero-shot skeleton-based action recognition via mutual information estimation and maximization. In *Proceedings of the ACM international conference on multimedia*, pp. 5302–5310, 2023.

Yuxuan Zhou, Xudong Yan, Zhi-Qi Cheng, Yan Yan, Qi Dai, and Xian-Sheng Hua. Blockgcn: Redefine topology awareness for skeleton-based action recognition. In *Proceedings of the IEEE/CVF Conference on Computer Vision and Pattern Recognition*, pp. 2049–2058, 2024b.

Anqi Zhu, Jingmin Zhu, James Bailey, Mingming Gong, and Qiuhong Ke. Semantic-guided cross-modal prompt learning for skeleton-based zero-shot action recognition. In *Proceedings of the Computer Vision and Pattern Recognition Conference*, pp. 13876–13885, 2025.

Wentao Zhu, Xiaoxuan Ma, Zhaoyang Liu, Libin Liu, Wayne Wu, and Yizhou Wang. Motionbert: A unified perspective on learning human motion representations. In *Proceedings of the IEEE/CVF International Conference on Computer Vision*, pp. 15085–15099, 2023a.

Wentao Zhu, Xiaoxuan Ma, Dongwoo Ro, Hai Ci, Jinlu Zhang, Jiaxin Shi, Feng Gao, Qi Tian, and Yizhou Wang. Human motion generation: A survey. *IEEE Transactions on Pattern Analysis and Machine Intelligence*, 46(4):2430–2449, 2023b.

APPENDIX

In this appendix, we provide additional materials to complement the main text. Specifically, we include detailed mathematical derivations (Appendix A), implementation details (Appendix B), supplementary quantitative results (Appendix C), additional qualitative results (Appendix D), user study information (Appendix E), and examples of HumanML3D annotations (Appendix F). These materials aim to facilitate a deeper understanding of our methodology and to support reproducibility of the experiments.

A MATHEMATICAL DERIVATIONS

A.1 AUTOREGRESSIVE MOTION DIFFUSION WITH ODE SAMPLING

Our diffusion model is based on the continuous-time probability flow ODE formulation. The process transforms a simple prior distribution $\pi(\mathbf{z}_{\mathrm{m},1}) = \mathcal{N}(0, \mathbf{I})$ into a complex data distribution $p_0(\mathbf{z}_{\mathrm{m},0})$.

Forward Process (Probability Flow ODE):
The forward process defines a trajectory from a data point $\mathbf{z}_{\mathrm{m},0}$ to a noise vector $\mathbf{z}_{\mathrm{m},1}$. We use a linear interpolation path, where the state at time $t \in [0, 1]$ is:

$$\mathbf{z}_{\mathrm{m},t} = (1-t)\mathbf{z}_{\mathrm{m},0} + t\boldsymbol{\epsilon}, \quad \text{where } \boldsymbol{\epsilon} \sim \mathcal{N}(0, \mathbf{I}) \tag{A1}$$

The probability density $p_t(\mathbf{z}_{\mathrm{m},t})$ of the variable $\mathbf{z}_{\mathrm{m},t}$ follows the continuity equation. The velocity field of this probability flow is given by the time derivative of the path:

$$\mathbf{v}(\mathbf{z}_{\mathrm{m},t}) = \frac{d\mathbf{z}_{\mathrm{m},t}}{dt} = \boldsymbol{\epsilon} - \mathbf{z}_{\mathrm{m},0} \tag{A2}$$

Our neural network $\mathbf{v}_\theta(\mathbf{h}, t)$ is trained to approximate this velocity field, conditioned on the context $\mathbf{h}$ from the MAR-Transformer. The training objective is to minimize the L2 loss:

$$\mathcal{L}_{\text{diff}} = \mathbb{E}_{\mathbf{z}_{\mathrm{m},0},\boldsymbol{\epsilon},t,\mathbf{h}} \left[\|\mathbf{v}_\theta(\mathbf{h}, t) - (\boldsymbol{\epsilon} - \mathbf{z}_{\mathrm{m},0})\|^2 \right] \tag{A3}$$

Reverse Process (Generative Sampling):
To generate a sample, we solve the reverse-time ordinary differential equation (ODE) from $t = 1$ to $t = 0$. The generative ODE is defined by the learned velocity field:

$$\frac{d\mathbf{z}_{\mathrm{m},t}}{dt} = \mathbf{v}_\theta(\mathbf{h}, t) \tag{A4}$$

Starting with an initial sample from the prior distribution, $\mathbf{z}_{\mathrm{m},1} \sim \mathcal{N}(0, \mathbf{I})$, we can obtain the final data sample $\mathbf{z}_{\mathrm{m},0}$ by integrating this ODE:

$$\mathbf{z}_{\mathrm{m},0} = \mathbf{z}_{\mathrm{m},1} - \int_0^1 \mathbf{v}_\theta(\mathbf{h}, t)\, dt \tag{A5}$$

In practice, this integral is approximated numerically using a solver, such as the Euler method. For a discrete number of steps N, starting with $\mathbf{z}_{\mathrm{m},t_i}$ where $t_i = 1 - i/N$, the update rule is:

$$\mathbf{z}_{\mathrm{m},t_{i+1}} = \mathbf{z}_{\mathrm{m},t_i} - \frac{1}{N}\mathbf{v}_\theta(\mathbf{h}, t_i) \tag{A6}$$

Iterating this process from $i = 0$ to $N - 1$ yields the final sample $\mathbf{z}_{\mathrm{m},0}$.

A.2 DERIVATION OF THE SEMANTIC GUIDANCE GRADIENT

The semantic guidance mechanism modifies the reverse sampling process by incorporating the gradient of a semantic alignment score $\mathcal{S}$. This can be viewed as sampling from a modified probability distribution that is a product of the original diffusion model's distribution and a guidance distribution.

Modified Generative Process:
Let $p_t(\mathbf{z}')$ be the probability density at time t induced by the unconditional diffusion model. We

introduce a guidance distribution $p_{\text{guide}}(\mathbf{z}') \propto \exp(\mathcal{S}(\mathcal{D}(\mathbf{z}'), c))$ that assigns higher probability to samples with better text-motion alignment. The new, guided distribution $p_{\text{guided}}(\mathbf{z}')$ is proportional to their product:

$$p_{\text{guided}}(\mathbf{z}') \propto p_t(\mathbf{z}') \cdot p_{\text{guide}}(\mathbf{z}')$$

Taking the logarithm:

$$\log p_{\text{guided}}(\mathbf{z}') = \log p_t(\mathbf{z}') + \mathcal{S}(\mathcal{D}(\mathbf{z}'), c) + \text{const.} \tag{A7}$$

The score function of a distribution is the gradient of its log-probability, $\nabla \log p$. Therefore, the score function of the guided distribution is:

$$\nabla_{\mathbf{z}'} \log p_{\text{guided}}(\mathbf{z}') = \nabla_{\mathbf{z}'} \log p_t(\mathbf{z}') + \nabla_{\mathbf{z}'} \mathcal{S}(\mathcal{D}(\mathbf{z}'), c) \tag{A8}$$

In score-based diffusion models, the score function is related to the predicted noise or velocity. For the flow-matching ODE, the velocity field can be seen as a proxy for the score. Thus, we can modify the original velocity field $\mathbf{v}_\theta$ by adding a term proportional to the gradient of the alignment score. The guided velocity field $\mathbf{v}_{\text{guided}}$ becomes:

$$\mathbf{v}_{\text{guided}}(\mathbf{h}, t) = \mathbf{v}_\theta(\mathbf{h}, t) + \gamma \cdot \nabla_{\mathbf{z}'} \mathcal{S}(\mathcal{D}(\mathbf{z}'), c) \tag{A9}$$

where γ is the guidance scale.

Chain Rule for Gradient Computation:

The gradient term $\mathbf{g} = \nabla_{\mathbf{z}'} \mathcal{S}(\mathcal{D}(\mathbf{z}'), c)$ is computed using the chain rule. Let $\hat{\mathbf{X}} = \mathcal{D}(\mathbf{z}')$. The score $\mathcal{S}$ is a composite function $\mathcal{S}(\hat{\mathbf{X}}(z'))$.

$$\mathbf{g} = \frac{d\mathcal{S}}{d\mathbf{z}'} = \frac{\partial \mathcal{S}}{\partial \hat{\mathbf{X}}} \frac{\partial \hat{\mathbf{X}}}{\partial \mathbf{z}'} \tag{A10}$$

Let's break down the first term, $\frac{\partial \mathcal{S}}{\partial \hat{\mathbf{X}}}$. The score is:

$$\mathcal{S}(\hat{\mathbf{X}}, c) = \sum_{k \in \{f,j,b,m\}} w_k \cdot \text{sim}(R_\phi^k(\hat{\mathbf{X}}), E_{\text{text}}(c))$$

$$\mathcal{S}(\hat{\mathbf{X}}, c) = \sum_k w_k \frac{R_\phi^k(\hat{\mathbf{X}}) \cdot E_{\text{text}}(c)}{\|R_\phi^k(\hat{\mathbf{X}})\| \|E_{\text{text}}(c)\|} \tag{A11}$$

The gradient with respect to the motion $\hat{\mathbf{X}}$ is then:

$$\frac{\partial \mathcal{S}}{\partial \hat{\mathbf{X}}} = \sum_k w_k \cdot \nabla_{\hat{\mathbf{X}}} \left(\frac{R_\phi^k(\hat{\mathbf{X}}) \cdot E_{\text{text}}(c)}{\|R_\phi^k(\hat{\mathbf{X}})\| \|E_{\text{text}}(c)\|} \right) \tag{A12}$$

This involves the derivative of the cosine similarity and the Jacobian of the MAR's embedding function R_ϕ^k. The second term in Eq. (A10), $\frac{\partial \hat{\mathbf{X}}}{\partial \mathbf{z}'}$, is the Jacobian of the decoder network $\mathcal{D}$. While these terms have complex analytical forms, automatic differentiation libraries compute their product $\mathbf{g}$ efficiently via a single backpropagation pass. This computed gradient is then normalized and applied as per Equations 7 and 8 in the main text to steer the ODE sampling process.

B Implementation Details

Our experiments are conducted on two NVIDIA RTX 4090 GPUs. The multimodal autoencoder (AE) comprises an encoder and a decoder, both based on the ResNet architecture. It first embeds the three modalities using 1D convolutional layers and then performs early fusion before feeding the input into a shared encoder. The encoder downsamples the motion sequence by a factor of 4, mapping the input features into a 512-dimensional latent space ($D = 512$). The masked autoregressive Transformer consists of a 6-layer Transformer model with a latent dimension of 1024. For the diffusion model, we utilize a multilayer perceptron (MLP) architecture. All models are trained using the AdamW optimizer with a learning rate of 2×10^{-4}. The multimodal action recognizer (MAR) is also a Transformer-based model with an embedding space dimension of 512, trained using a contrastive loss with a temperature parameter $\tau = 0.1$. During inference, the guidance scale γ for semantic guidance is set to 1.0.

C SUPPLEMENTARY QUANTITATIVE RESULTS

D ADDITIONAL QUALITATIVE RESULTS

D.1 VISUALIZATIONS

We visualize motions generated by the original MLD (Chen et al., 2023) and by MLD fine-tuned with our EasyTune, as shown in Fig. 5. Our proposed EasyTune substantially improves the capacity of text-to-motion models to comprehend textual semantics. For example, in Fig. 5(j), the model fine-tuned with our proposed EasyTune effectively generates a motion that accurately reflects the semantic intent of the description “The man is marching like a soldier,” whereas the original model fails to capture this nuanced behavior.

APPENDIX

In this appendix, we provide additional materials to complement the main text. Specifically, we include detailed mathematical derivations (Appendix A), implementation details (Appendix B), supplementary quantitative results (Appendix C), additional qualitative results (Appendix D), user study information (Appendix E), and examples of HumanML3D annotations (Appendix F). These materials aim to facilitate a deeper understanding of our methodology and to support reproducibility of the experiments.

A MATHEMATICAL DERIVATIONS

B IMPLEMENTATION DETAILS

C SUPPLEMENTARY QUANTITATIVE RESULTS

D ADDITIONAL QUALITATIVE RESULTS

D.1 VISUALIZATIONS

We visualize motions generated by the original MLD (Chen et al., 2023) and by MLD fine-tuned with our EasyTune, as shown in Fig. 5. Our proposed EasyTune substantially improves the capacity of text-to-motion models to comprehend textual semantics. For example, in Fig. 5(j), the model fine-tuned with our proposed EasyTune effectively generates a motion that accurately reflects the semantic intent of the description “The man is marching like a soldier,” whereas the original model fails to capture this nuanced behavior.

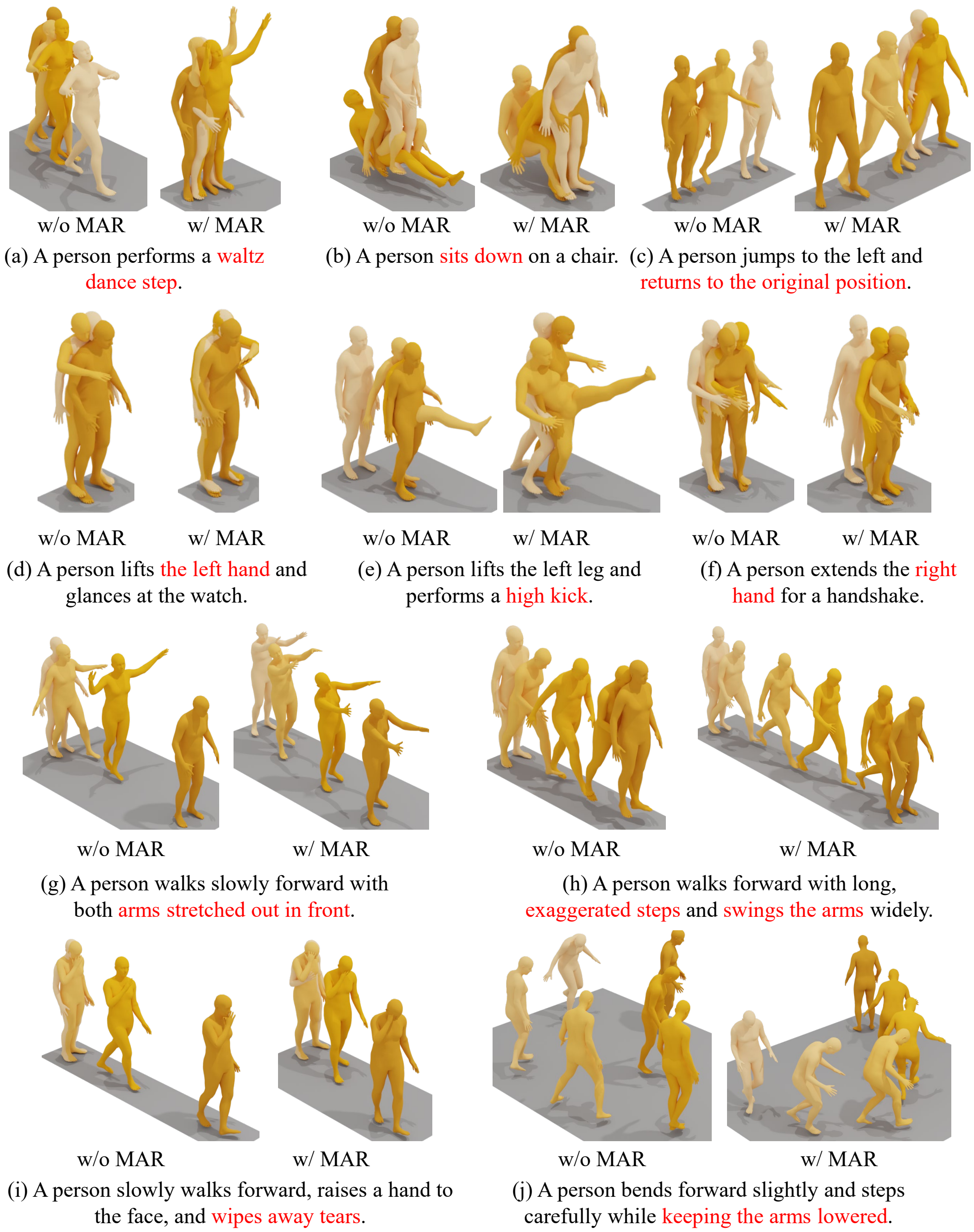

Figure 4: Visual results on HumanML3D dataset. "w/o EasyTune" refers to motions generated by the original MLD model (Chen et al., 2023), while "w/ EasyTune" indicates motions generated by the MLD model fine-tuned using our proposed EasyTune.

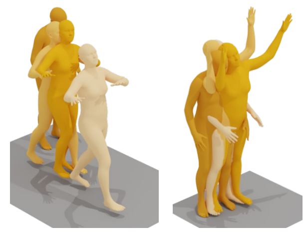

w/o MAR w/ MAR

(a) A person performs a waltz dance step.

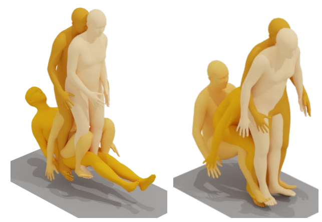

w/o MAR w/ MAR

(b) A person sits down on a chair.

w/o MAR w/ MAR

(c) A person jumps to the left and returns to the original position.

w/o MAR w/ MAR

(d) A person lifts the left hand and glances at the watch.

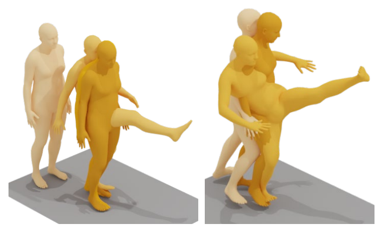

w/o MAR w/ MAR

(e) A person lifts the left leg and performs a high kick.

w/o MAR w/ MAR

(f) A person extends the right hand for a handshake.

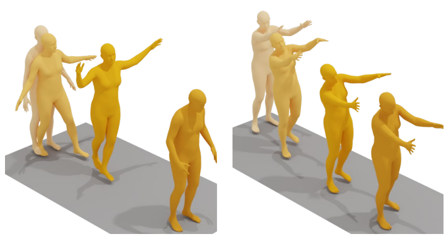

w/o MAR w/ MAR

(g) A person walks slowly forward with both arms stretched out in front.

w/o MAR w/ MAR

(h) A person walks forward with long, exaggerated steps and swings the arms widely.

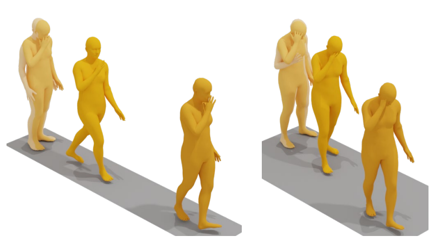

w/o MAR w/ MAR

(i) A person slowly walks forward, raises a hand to the face, and wipes away tears.

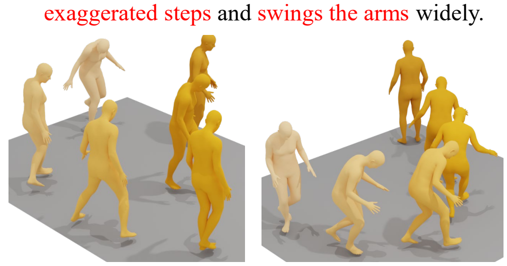

w/o MAR w/ MAR

(j) A person bends forward slightly and steps carefully while keeping the arms lowered.

Figure 5: Visual results on HumanML3D dataset. “w/o EasyTune” refers to motions generated by the original MLD model (Chen et al., 2023), while “w/ EasyTune” indicates motions generated by the MLD model fine-tuned using our proposed EasyTune.